Graphitic carbon nitride (g-C_3N_4) as an efficient metal-free Fenton-like catalyst for degrading organic pollutants: the overlooked non-photocatalytic activity

G. X. Zhu, T. L. Lu, L. Han and Y. Z. Zhan

ABSTRACT

Graphitic carbon nitride (g-C_3N_4) has attracted a large amount of research, mainly being used as a photocatalyst, but its Fenton-like catalytic performance has been overlooked. In this paper, the dark Fenton-like catalytic performance of g-C_3N_4 was evaluated by degrading rhodamine B over a wide pH range. The results showed that the g-C_3N_4, which was synthesized by conventional urea pyrolysis without any modification, was an efficient metal-free heterogeneous Fenton-like catalyst. The highest activity occurred under a weakly alkaline condition of about pH 10. The experiment of catalyst recycling indicated that g-C_3N_4 had long-term stability. The reactive oxidizing species of HO·, generated by the g-C_3N_4 activating H_2O_2, was identified by EPR and further supported by a scavenging experiment of HO· using isopropanol as the scavenger. The HNO_3 oxidation of g-C_3N_4 resulted in catalytic deactivation, implying the catalytic activity originated from the surface reduced groups of g-C_3N_4. The structure of synthesized g-C_3N_4 before and after the HNO_3 oxidation was characterized by X-ray diffraction, Fourier transform infrared spectroscopy, and X-ray photoelectron spectroscopy, and a possible catalytic mechanism was proposed.

Key words | graphitic carbon nitride, heterogeneous Fenton-like reaction, hydroxyl radical, metal-free catalyst, organic pollutant, wastewater treatment

G. X. Zhu
T. L. Lu
Y. Z. Zhan (corresponding author)
School of Chemical Engineering,
Zhengzhou University,
Zhengzhou 450001,
China
E-mail: *zhanyz@zzu.edu.cn*

L. Han
School of Ecology and Environment,
Zhengzhou University,
Zhengzhou 450001,
China

INTRODUCTION

Although the classical homogeneous Fenton reaction, in which highly aggressive hydroxyl radicals (HO·) are generated from H_2O_2 by the redox cycle of Fe^{2+}/Fe^{3+}, has been used for the degradation of recalcitrant organic pollutants, some drawbacks hamper the wider application of this process. For example, this process only works at acidic pH (2.5–3), and Fe^{2+} ions result in formation of iron sludge, which has to be removed and hence increases the operation cost. To overcome these disadvantages, much attention has been paid to heterogeneous Fenton-like systems in recent decades (Zhu *et al.* 2019). Naturally, the research mainly focuses on Fe-containing solids (Wu *et al.* 2015; Hammedi *et al.* 2019; Zhu *et al.* 2019), and then extends to various Cu-containing materials (Dong *et al.* 2015; Lyu *et al.* 2015; Zhang *et al.* 2017; Su *et al.* 2019). Other non-iron materials, such as Ag, Al, Ce, Co, Cr, Mn, Au, and Ru, have also been investigated (Bokare & Choi 2014). Many of these solid catalysts with metals as active species show fairly high catalytic activity; however, their imperfect stability is still a major barrier impeding their commercial applications (Zhu *et al.* 2019). In heterogeneous Fenton-like processes, the leaching of metal ions caused by acidity and complexation is almost inevitable, resulting in a rapid deactivation of these catalysts. To avoid this deactivation, metal-free materials, especially carbon materials, have received increasing interest in recent years (Ribeiro *et al.* 2016). Carbon materials studied as heterogeneous Fenton-like catalysts on their own include activated carbon, carbon xerogel, carbon black, glycerol-based carbon, biochar, carbon nanotube, carbon quantum dot, graphite, and graphene. The catalytic activity was generally attributed to the basic oxygen-containing functional groups of these carbon materials. These groups activated H_2O_2, generating HO· by redox cycles, similar to the redox cycle of Fe^{2+}/Fe^{3+} in the classical Fenton process (Espinosa *et al.* 2015; Navalon *et al.* 2017; Vega & Valdés 2018). Among these carbon materials, graphene, a famous 2D

doi: 10.2166/wst.2020.129

carbon material, has attracted the most intensive attention, mainly due to its tremendous specific surface areas, high chemical stability, superior electron mobility, abundant oxygen-containing functional groups, and easy-to-modulate active sites. Graphene (Espinosa *et al.* 2015), graphene oxide (GO) (Ribeiro *et al.* 2016; Zhao *et al.* 2017), and reduced graphene oxide (r-GO) (Espinosa *et al.* 2015) were all studied as heterogeneous metal-free catalysts for Fenton-like processes. r-GO usually exhibited the highest catalytic activity, while GO exhibited the lowest (Espinosa *et al.* 2015). This is because the type and the number of surface oxygen-containing functional groups markedly influenced their catalytic performance. Basic oxygen-containing functional groups were reductive and might transfer electrons to H_2O_2, generating HO·. In contrast, oxidative oxygen-containing functional groups caused invalid decomposition of H_2O_2. This invalid decomposition resulted in a decrease not only in the utilization of H_2O_2 but also in the catalytic activity. To modulate the surface functional groups of carbon materials, doping heteroatoms is an effective strategy. Nitrogen is the most widely studied heteroatom in doped graphenes as well as other carbon materials (Kong *et al.* 2014). Doping nitrogen on carbon materials usually enhanced their Fenton-like catalytic activity (Martin-Martinez *et al.* 2016; Granzier-Nakajima *et al.* 2019).

Graphitic carbon nitride (g-C_3N_4) is another famous 2D carbon material, which has a similar structure to graphene but containing nitrogen. Mainly as a photocatalytic material, g-C_3N_4 has attracted increasing interest in recent years (Mamba & Mishra 2016; Ong *et al.* 2016; Kumar *et al.* 2018). g-C_3N_4 contains not only plenty of nitrogen-containing but also some oxygen-containing functional groups. This material is easy to synthesize on a large scale with various cheap raw materials, and also easy to modify by various strategies (Reddy *et al.* 2019). Curiously, it seems that this material has never been studied as a Fenton-like catalyst. In fact, in many studies dealing with g-C_3N_4 as photo-Fenton catalysts or as supports of Fenton-like catalysts, controlled experiments of g-C_3N_4 as Fenton-like catalysts were always carried out to illustrate the low activity of g-C_3N_4 (Table S1, Supplementary Information). In this study, we using rhodamine B (RhB) as a simulated organic pollutant to evaluate the Fenton-like catalytic performance of g-C_3N_4 over a wide pH range. We found that even the unmodified g-C_3N_4 synthesized by conventional urea pyrolysis was still an efficient heterogeneous Fenton-like catalyst.

METHODS

Materials

Urea was purchased from Tianjin Fengchuan Chemical Reagent Co., Ltd (Tianjin, China). RhB was purchased from Sinopharm Chemical Reagent Co., Ltd (Shanghai, China). H_2O_2 (30%), HCl (36%), and NaOH were purchased from Shanghai Wokai Biotechnology Co., Ltd (Shanghai, China). All these reagents are of analytical grade.

Preparation of g-C_3N_4

g-C_3N_4 was synthesized by the conventional urea pyrolysis (Liu *et al.* 2011). Urea in a crucible with a cover was dried at 80 °C for 1 h. Then the crucible was put in a muffle furnace, heated to 580 °C with the heating rate of about 3 °C min^{-1}, and remained at 580 °C for 3 h to complete the reaction. The yellow product obtained was washed in turn with 0.1 mol L^{-1} HCl, deionized water, and ethanol until the filtrate was neutral. Lastly, the wet sample was dried in a vacuum freeze dryer for 10 h.

Characterization of g-C_3N_4

X-ray diffraction (XRD) data were collected on a Bruker D8 Advance diffractometer with Cu K_α radiation. Fourier transform infrared (FTIR) spectra were obtained on a Bruker Tenser II infrared spectrophotometer using the KBr disc method. Scanning electron microscopy (SEM) images were recorded on a Hitachi S2400 scanning electron microscope. X-ray photoelectron spectroscopy (XPS) measurements were conducted on a Thermo Scientific-Escalb 250XI electron spectrometer. The specific surface area was obtained according to the Brunauer–Emmett–Teller (BET) method from the nitrogen adsorption at liquid nitrogen temperature using a Qutantachrome NOVA 2000e system.

Catalytic evaluation of g-C_3N_4

To evaluate the catalytic performance of the g-C_3N_4, 100 mL RhB solution with a concentration of 20 mg L^{-1} was used as simulated wastewater. The degradation of RhB was carried out in a glass reactor of 250 mL immersed in a constant temperature water bath with magnetic stirring. The initial solution pH was adjusted using a small amount of 0.1 mol L^{-1} HCl or 0.1 mol L^{-1} NaOH solution. After adding

20 mg g-C_3N_4 into the RhB solution, the mixture was stirred for 30 min to achieve adsorption–desorption equilibrium. Then the reaction was started by adding a certain amount of H_2O_2 solution. All reactions were carried out at 50 °C, pH 10, and 100 mmol L^{-1} H_2O_2 unless noted otherwise. At predetermined time intervals, a 4 mL reaction solution was taken out. After immediate centrifugation, the concentration of RhB was analyzed at 554 nm using an INESA 722G spectrophotometer. The UV-vis absorption spectra of the reaction solution were recorded by using a Shimadzu UV-1780 spectrophotometer.

The electron paramagnetic resonance (EPR) spectra were recorded on an EPR spectrometer (EMX Plus, Bruker, Germany). 5,5-dimethyl-1-pyrroline N-oxide (DMPO) was used as a radical trapping agent.

RESULTS AND DISCUSSION

Characterization of g-C_3N_4

XRD and FTIR were used to verify the crystal structure and surface characteristics of the synthesized g-C_3N_4 product. The results were in good accordance with the data reported previously (Figure 1) (Liu *et al.* 2011; Wang *et al.* 2019). The strong XRD peak at 27.5° was indicative of the graphitic stacking structure, which was indexed as (002). Another obvious peak at 13.1° was attributed to the in-planar repeating unit, which was indexed as (100). The FTIR spectrum of the product demonstrated the graphitic structures further. The wide band between 3,000 and 3,500 cm^{-1} was attributed to N–H stretching vibration modes, indicating that uncondensed amino groups still existed in the product. The strong bands at 1,630, 1,569, 1,454, and 1,395 cm^{-1} were assigned to stretching vibration modes of heptazine-derived repeating units. The sharp band at 808 cm^{-1} represented the out-of-plane bending vibration of heptazine rings. The bands at 1,313 and 1,229 cm^{-1} corresponded to stretching vibration of connected units of $N–(C)_3$ or C–NH–C. The SEM image of the synthesized product presented a sheet structure with a thin thickness, which was similar to the morphology of g-C_3N_4 synthesized using similar methods (Lu *et al.* 2016; Yue *et al.* 2016; Yang *et al.* 2017). The nitrogen adsorption–desorption isotherm of the synthesized product showed the type IV isotherm. The specific surface area was calculated according to BET theory as 77 $m^2 g^{-1}$, which was also near the values of g-C_3N_4 synthesized using similar methods (Liu *et al.* 2011; Sudhaik *et al.* 2018).

Effect of initial pH on catalytic activity of g-C_3N_4

The initial pH value of wastewater usually strongly affects the degradation of organic pollutants in Fenton or Fenton-like processes, whether in homogeneous or heterogeneous systems. Catalysts usually have high activity only in a relatively narrow pH range. In most cases, the optimum pH range is weak acidity, and for some catalysts, the optimum pH can be extended to neutrality. Few catalysts have activity in the alkaline range. The Fenton-like catalytic activity of the g-C_3N_4 was also strongly influenced by the initial pH value, as shown in Figure 2. The g-C_3N_4 had the lowest catalytic activity at pH 4, and when pH was less than 4 the catalytic activity increased slightly. However, when the pH was greater than 4, the catalytic activity of the g-C_3N_4 obviously increased with the pH increase. That is to say, the catalytic activity of the g-C_3N_4 was the highest under alkaline conditions (around pH 10). To eliminate the influence of the non-catalytic degradation of H_2O_2, a controlled experiment was carried out in the same pH range. The results showed that without catalytic activation H_2O_2 itself is indeed a rather weak oxidant, although the non-catalytic degradation of RhB increased slightly with the increase of pH. For example, at pH 10, the non-catalytic degradation was only 27% in 140 min, and the catalytic degradation of RhB reached 92%. This clearly proved that the g-C_3N_4 had a high heterogeneous Fenton-like catalytic activity. On the other hand, we can get the rate constants by fitting the experimental data with the first-order kinetic equation. The rate constant was 0.00209 min^{-1} for the non-catalytic degradation, but it was 0.0184 min^{-1} for the catalytic degradation, which increased about nine times. This rate constant also showed that the Fenton-like catalytic activity of g-C_3N_4 was fairly good, especially when considering the dosage of g-C_3N_4 as low as 0.2 g L^{-1}.

It should be pointed out that our experiments showed that g-C_3N_4 had only lower Fenton catalytic activity under weak acidic to neutral condition. This condition was usually the optimized pH range for Fenton and photo-Fenton studies. Furthermore, the natural pH of dye solutions commonly used as pollutant models is usually weak acidic or neutral if the pH value is not adjusted. This may be one of the reasons for the low activity of g-C_3N_4 as Fenton catalysts observed in the controlled experiments reported in the literature (Table S1).

Effect of reaction temperature on catalytic activity of g-C_3N_4

At room temperature, the Fenton catalytic activity of the g-C_3N_4 was undistinguished, which may be another reason

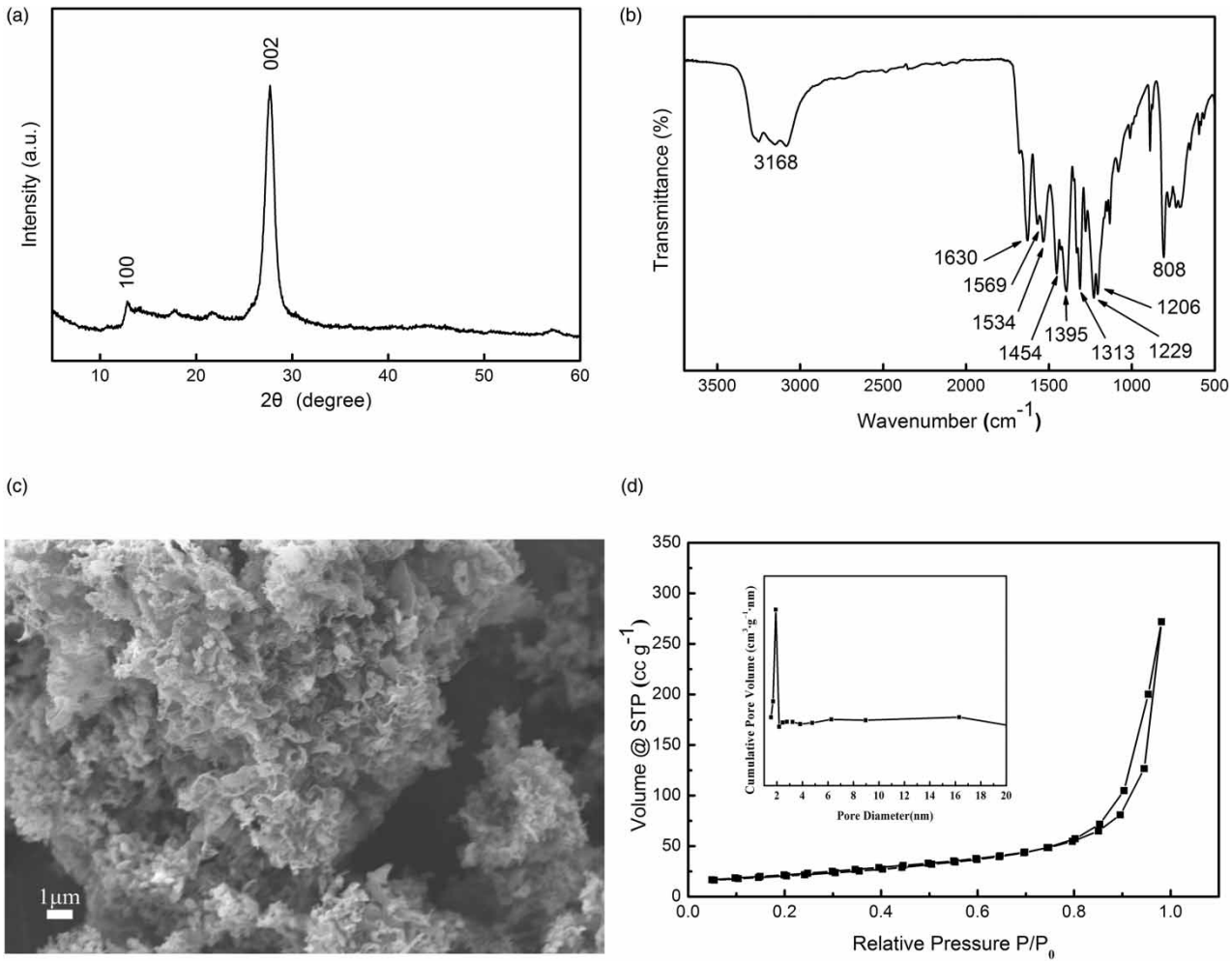

Figure 1 | Characterization of the synthesized product. (a) XRD pattern, (b) FTIR spectrum, (c) SEM image, and (d) nitrogen adsorption–desorption isotherm (insert: pore-size distribution).

for its neglect with regard to catalytic performance. As shown in Figure 3, at 30 °C the degradation of RhB was only about 40% in 140 min. Increasing the temperature can expectedly enhance the catalytic activity of the g-C_3N_4. At 60 °C the degradation of RhB could reach 96% in 140 min. At 70 °C the degradation in 20 min reached 83%. Correspondingly, the rate constant of the first-order reaction increased from 0.00300 min^{-1} at 30 °C to 0.0706 min^{-1} at 70 °C, which was about 23 times higher. The rate constants at different temperatures agreed well with the Arrhenius equation (Table S2, Figure S1, Supplementary Information), and the apparent activation energy of degradation calculated was 65.6 kJ mol^{-1}.

Effect of H_2O_2 concentration on catalytic activity of g-C_3N_4

As oxidant, the concentration of H_2O_2 strongly affected the degradation of RhB (Figure 4, Table S3). When the concentration of H_2O_2 was 40 mmol L^{-1}, the degradation of RhB was only about 43.1% in 140 min, and when the concentration was 100 mmol L^{-1}, the degradation reached 93.4% in the same time. Correspondingly, the rate constant of the first-order reaction increased from 0.00380 to 0.0184 min^{-1}, which was about four times higher. Further increasing the concentration of H_2O_2 had no contribution to improving the degradation.

The theoretical requirement for H_2O_2 for mineralizing RhB can be calculated according to the following stoichiometric equation (Gu *et al.* 2019):

$$C_{28}H_{31}ClN_2O_3 + 73H_2O_2 \rightarrow 28CO_2 + 87H_2O + 2HNO_3 + HCl \quad (1)$$

It can be calculated that the concentration of H_2O_2 should be 2.92 mmol L^{-1} for mineralizing RhB of 20 mg L^{-1} (corresponding to 0.04 mmol L^{-1}). Thus, an

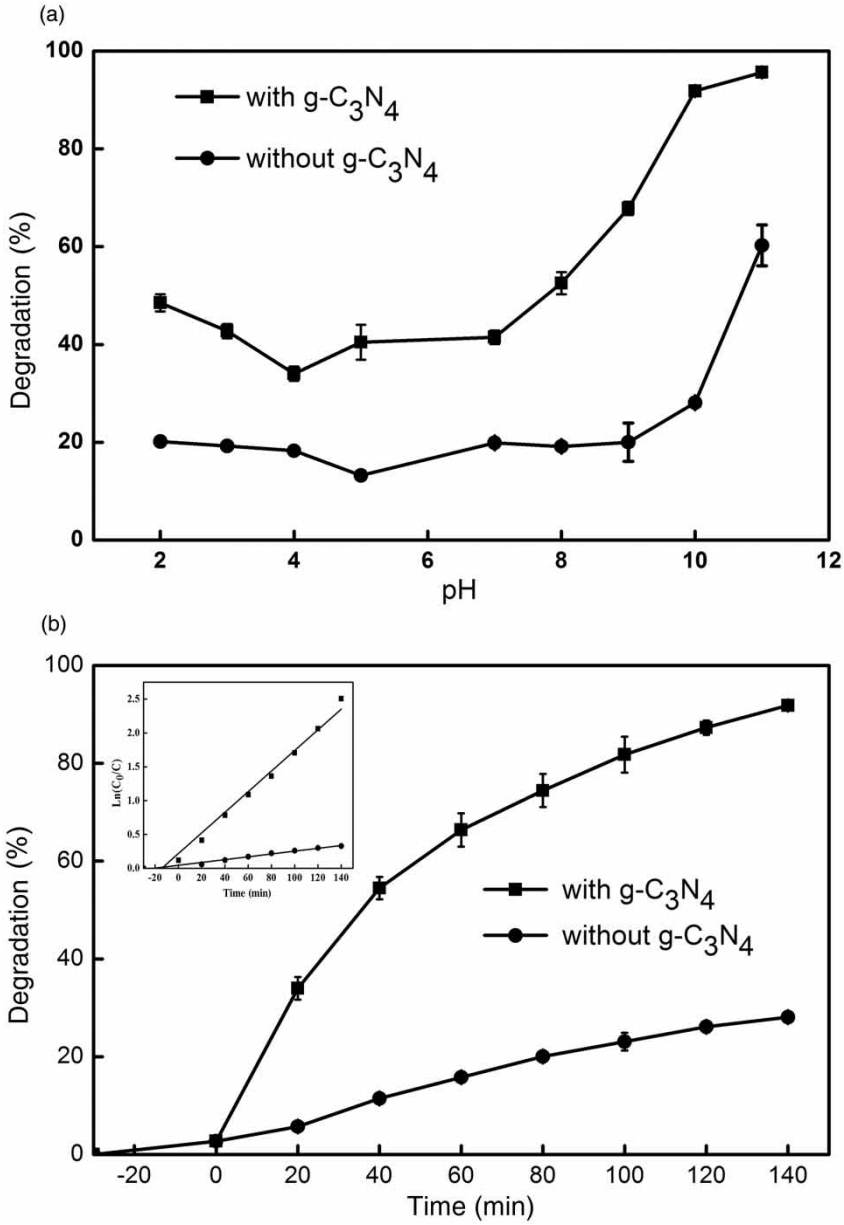

Figure 2 | (a) Effect of initial pH on RhB degradation (140 min). (b) RhB degradation at pH = 10 (insert: fitting of the first-order kinetic equation).

H_2O_2 concentration of 100 mmol L^{-1} is 34 times the theoretical amount, indicating relatively lower utilization of H_2O_2 in this system. To achieve higher degradation at low H_2O_2 concentration, a longer time or higher temperature is needed. It also shows that g-C_3N_4 as a Fenton-like catalyst still should be improved.

Stability of g-C_3N_4

As a metal-free material, it is expected that g-C_3N_4 exhibits better stability because there is no leaching problem of metal ions. Its stability was tested by separating the catalyst from the Fenton-like system after the reaction and repeatedly using it. No significant decrease in catalytic activity was observed after five cycles as shown in Figure 5, indicating that the g-C_3N_4 had good repeatability and long-term stability.

Study of catalytic mechanism

The reactive oxidizing species of HO· was confirmed by EPR, as shown in Figure 6. Using DMPO as the radical trapping agent, the characteristic EPR spectrum of

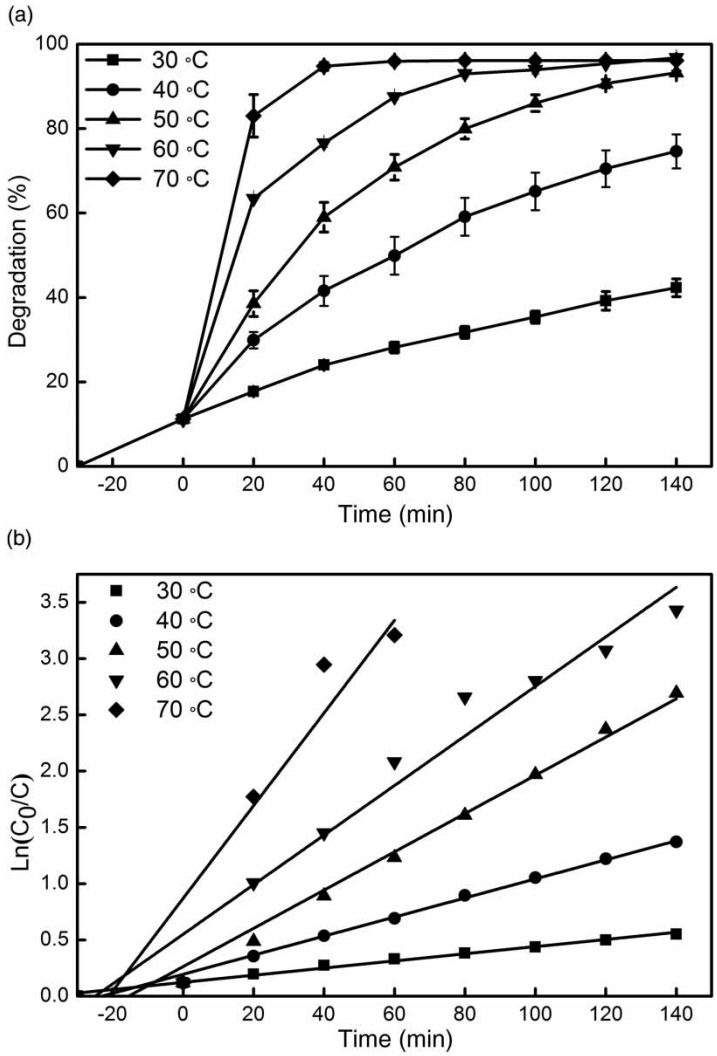

Figure 3 | (a) Effect of temperatures on RhB degradation. (b) Fitting of the first-order kinetic equation at different temperatures.

the DMPO-OH spin adduct was recorded in the g-C_3N_4/H_2O_2 system. However, without g-C_3N_4 the spectrum was very weak. These results clearly demonstrated that g-C_3N_4 activated H_2O_2, generating HO·. That HO· was the major reactive oxidizing species was further supported by a scavenging experiment of free radicals, in which the addition of isopropanol, an HO· scavenger, significantly decreased the degradation of RhB (Figure 7). Highly active HO· can quickly destruct the structure of the xanthene-conjugated chromophore (554 nm) of the RhB molecule, as shown in the UV–vis spectra of the reaction solution (Figure 8) (Lee *et al.* 2016). The superoxide radicals and non-catalytic oxidation of H_2O_2 may also contribute to the degradation of the dye because the addition of isopropanol did not completely inhibit the degradation (Figure 7).

Deep studies on the mechanism of catalysis are difficult and challenging work. Here we only propose a possible catalytic mechanism to explain the experimental results. In the classical Fenton process, H_2O_2 is activated by the redox cycle of Fe^{2+}/Fe^{3+} generating active free radical species, mainly HO·. Similarly, the activation of H_2O_2 by the redox cycle of surface reduced/oxidized states of carbon materials was also employed to explain the catalytic mechanism of carbon materials as Fenton-like catalysts (Espinosa *et al.* 2015; Navalon *et al.* 2017; Vega & Valdés 2018). We think that g-C_3N_4 activated H_2O_2 also through a similar pathway:

$$CN + H_2O_2 \rightarrow CN^+ + HO^- + HO \quad (2)$$

$$CN^+ + H_2O_2 \rightarrow CN + HO_2\cdot + H^+ \quad (3)$$

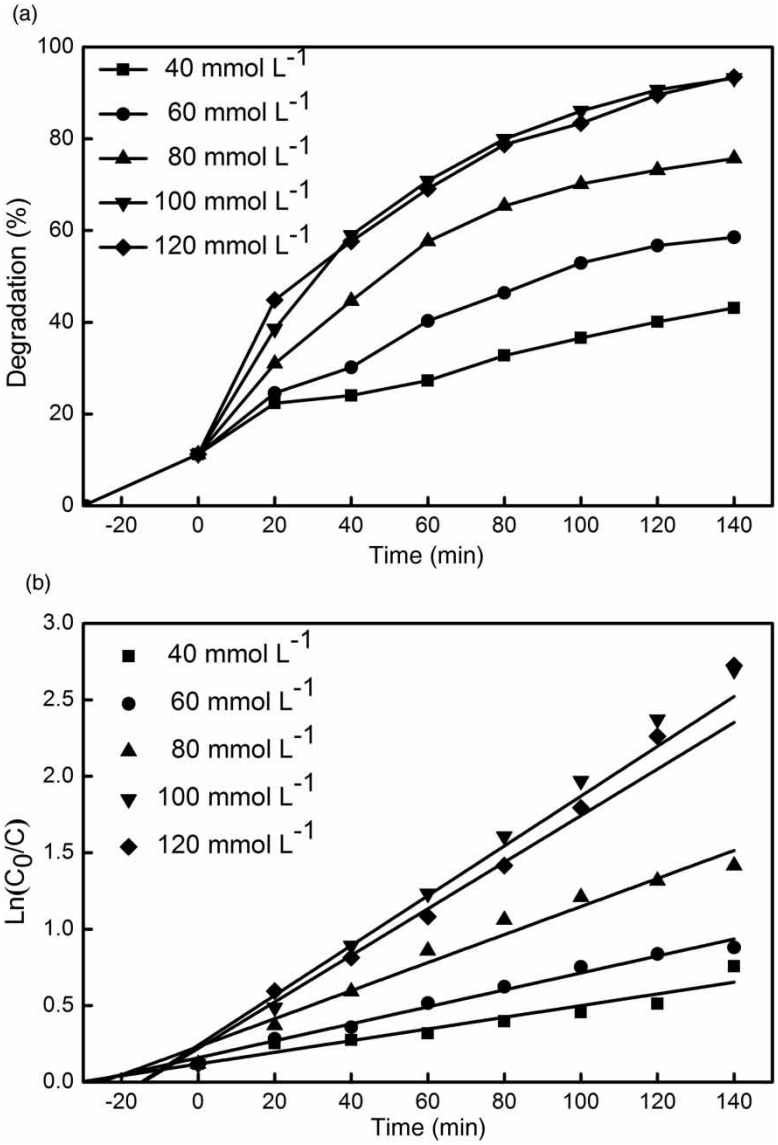

Figure 4 | (a) Effect of H_2O_2 concentration on RhB degradation. (b) Fitting of the first-order kinetic equation at different H_2O_2 concentrations.

By transferring a single electron from an active site of g-C_3N_4 to H_2O_2, the reduced catalyst states of CN activated H_2O_2, generating HO· and CN^+, the oxidized catalyst states, and then the CN^+ was reduced by H_2O_2, regenerating CN. Based on the above mechanism, we can also reasonably explain the effect of initial pH on the degradation performance. The active sites of g-C_3N_4 should be Lewis base functional groups with rich electrons. These groups prefer to accept protons under acidic conditions, inhibiting their ability to activate H_2O_2. Therefore, g-C_3N_4 showed higher catalytic activity under basic conditions.

The reducibility of active sites was supported by a preliminary experiment. After oxidation by HNO_3, the g-C_3N_4 almost completely lost its Fenton-like catalytic activity (Figure 7). In order to identify the specific active group, we compared the structure of g-C_3N_4 before and after HNO_3 oxidation by XRD, FTIR, and XPS characterization. The results are shown in Figure 9, Figure S2, and Table S4. After HNO_3 oxidation, the main peak (002) of the g-C_3N_4 XRD pattern showed only a decrease of the intensity and a slight shift towards higher angles (Figure S2), reflecting a possible disorder introduced in the graphitic planes by the oxidation process and a reduction of the inter-planar stacking distance (Pisanu *et al.* 2018). Comparing the FTIR spectra of the g-C_3N_4 before and after HNO_3 oxidation, we cannot observe the structural change resulting from the oxidation

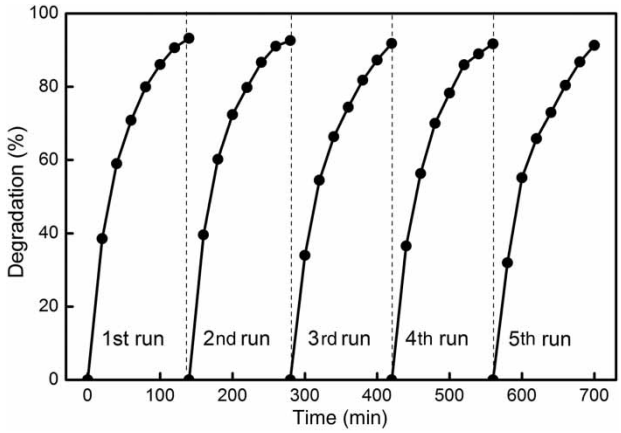

Figure 5 | Reuse of g-C_3N_4 for degrading RhB.

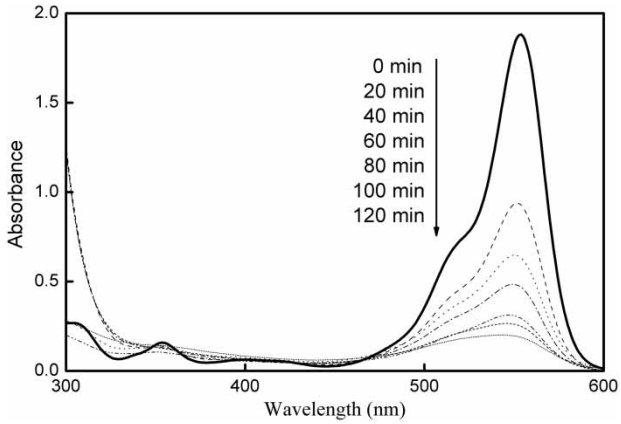

Figure 8 | UV–vis absorption spectra of reaction solution during RhB degradation.

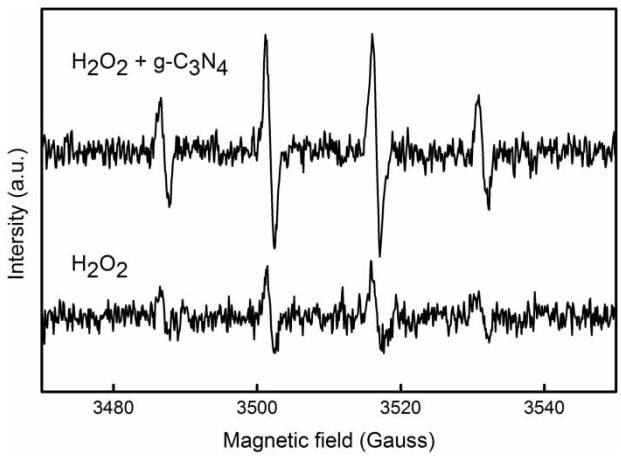

Figure 6 | EPR spectra of the DMPO-OH of H_2O_2 solution with and without g-C_3N_4.

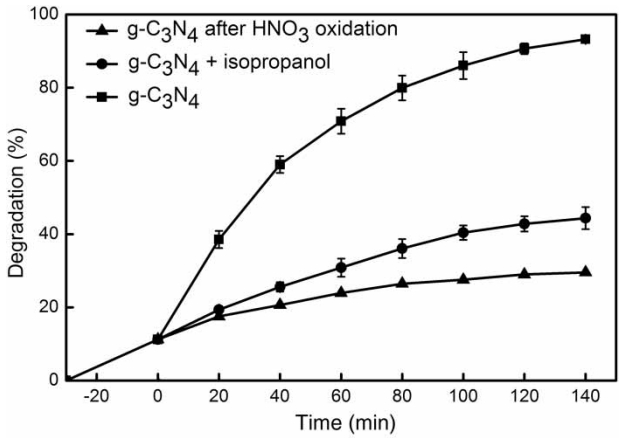

Figure 7 | Effect of adding isopropanol and oxidizing g-C_3N_4 by HNO_3 on RhB degradation.

(Figure S2). Although C=O and C–O groups are commonly formed in the process of g-C_3N_4 oxidation, it is difficult to detect them by the conventional FTIR technique, because these groups are usually present only on the surface of g-C_3N_4. The adsorption band of C=O vibration should appear at around 1,720 cm^{-1}; nevertheless there was no detectable absorption peak before and after the HNO_3 oxidation. The very weak peak at 1,080 cm^{-1}, which was attributed to C–N vibration, did not change observably after the oxidation. It is generally believed that the C–O bond and C–N bond have similar bond force constants; the weak C–O absorption can hardly cause the observable change of the 1,080 cm^{-1} peak (Li *et al.* 2015; Yang *et al.* 2017; Pisanu *et al.* 2018).

XPS is a surface-sensitive technique that easily detects changes of the catalyst surface groups (Figure 9). The XPS spectrum of pristine g-C_3N_4 presented characteristics of the common g-C_3N_4. The survey scan of the XPS spectrum showed that the synthesized product was composed primarily of carbon and nitrogen. The very weak O1s peak may come from adsorbed oxygen, which was commonly observed in XPS spectra of g-C_3N_4. The high-resolution spectrum of C1s showed the deconvoluted two peaks at 288.0 and 284.8 eV. The major peak at 288.0 eV corresponded to sp2-bonded carbon (N–C=N), and the weaker one at 284.8 eV was attributed to graphitic carbon, which usually appears on the XPS characterization for g-C_3N_4. The high-resolution spectrum of N1s showed the deconvoluted three peaks at 398.6, 400.2, and 401.3 eV. The main peak at 398.6 eV could be attributed to sp2 hybrid nitrogen (C–N=C). The peak at 400.2 eV was ascribed to tertiary nitrogen (N–$(C)_3$). The peak at 401.3 eV corresponded to amino groups with a hydrogen atom (C–N–H). After HNO_3 oxidation, an obvious enhanced O1s peak appeared in the XPS survey scan of the oxidized g-C_3N_4, indicating the oxidation resulted in formation of oxygen-containing groups. The high-resolution spectrum of O1s showed the

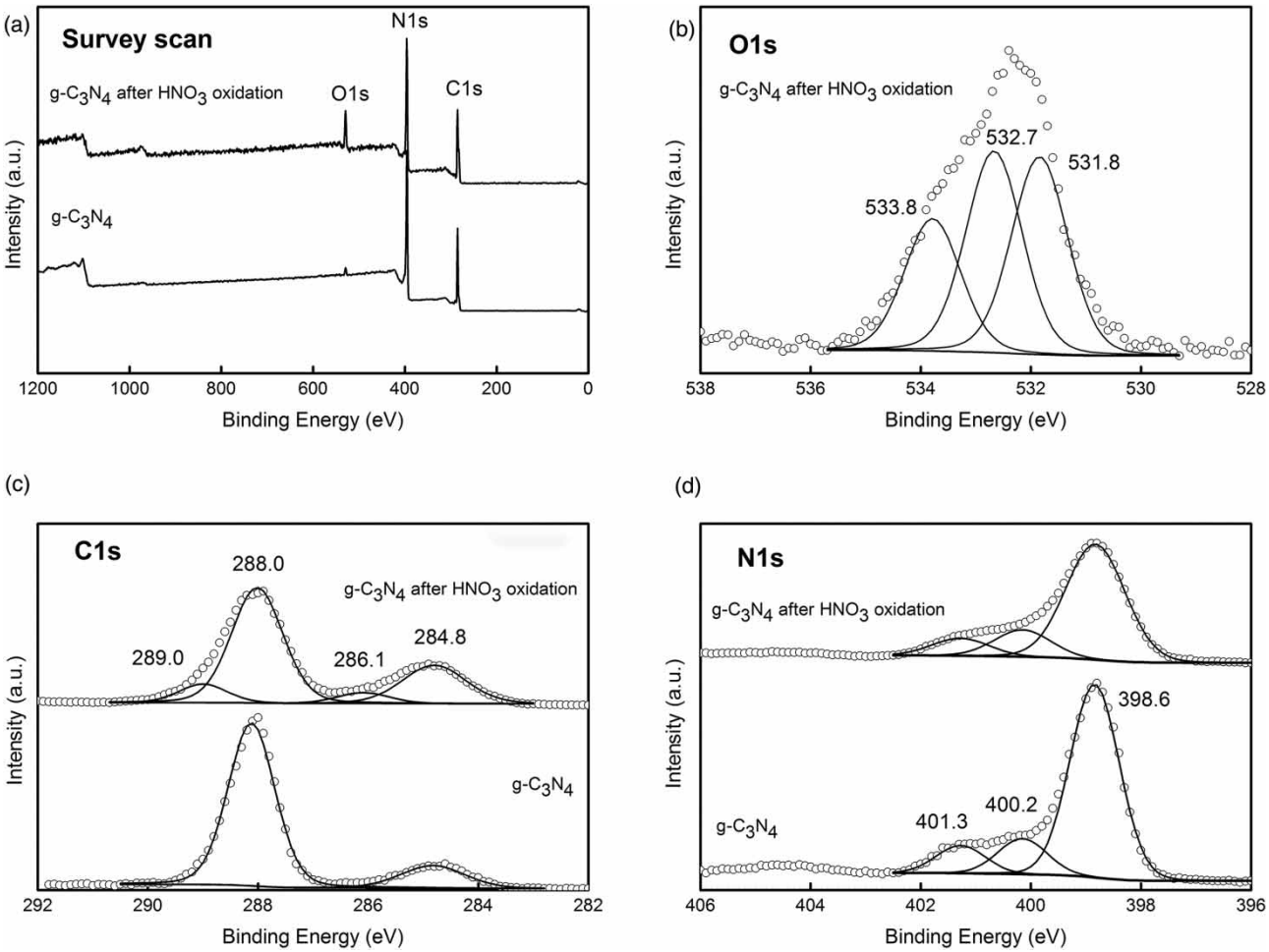

Figure 9 | XPS survey spectra (a), high-resolution XPS spectra of the O1s region (b), C1s region (c), and N1s region (d) of g-C_3N_4 before and after HNO_3 oxidation.

deconvoluted three peaks at 531.8, 532.7, and 533.8 eV, being attributed to oxygen of O=C, O–C and O–H, respectively. Accordingly, two new C1s peaks at 286.1 and 289.0 eV attributed to carbon of O–C and O=C–O, respectively, can be deconvoluted from the C1s high-resolution spectrum of the oxidized g-C_3N_4 (Li *et al.* 2015; Yang *et al.* 2017; Pisanu *et al.* 2018). However, after oxidation no new peaks appeared in the high-resolution spectrum of N1s, but the surface content of nitrogen decreased obviously and the N/C atomic ratio decreased from 1.32 (very close to the theoretical ratio 1.33) to 0.90 (Table S4), indicating that some of the nitrogen atoms were lost during the HNO_3 oxidation. Nevertheless, most of the nitrogen-containing groups remained, and the relative content did not change significantly.

Given the above discussion, it can be concluded that the oxidation process only introduced a certain amount of oxygen-containing groups but did not completely destroy the basic result of g-C_3N_4. This may indicate that the electron-rich triazine group was the active site for activating hydrogen peroxide. The HNO_3 oxidation, which introduced electron-withdrawing oxygen-containing groups, especially the carboxyl group, significantly changed the surface electron distribution of g-C_3N_4, resulting in catalyst deactivation. In addition, oxidative oxygen-containing functional groups may cause invalid decomposition of H_2O_2, resulting in a decrease not only in the utilization of H_2O_2 but also in the catalytic activity.

CONCLUSIONS

The photocatalytic performance of g-C_3N_4 has attracted extensive research, but its Fenton-like catalytic performance has been neglected. In this paper, it has been proved for the first time that g-C_3N_4 is an efficient and stable

heterogeneous Fenton-like catalyst, and its highest activity occurs in the alkaline condition of about pH 10. Like other carbon materials, it may activate H_2O_2 at the Lewis base site to produce HO·, thus degrading organic pollutants. Of course, the study of the mechanism is insufficient, and more evidence is needed for the identification of active groups. Also, the reaction activity is not high at room temperature and the consumption of H_2O_2 is relatively high. However, because g-C_3N_4 can be modified by various strategies and this material is easy to synthesize on a large scale with various cheap raw materials, g-C_3N_4 should be a potential candidate as excellent heterogeneous metal-free Fenton-like catalysts.

ACKNOWLEDGEMENTS

We are grateful to the National Natural Science Foundation of China (21802125) and the Henan Science and Technology Project (172102210490) for the financial support.

CONFLICT OF INTEREST

There are no conflicts to declare.

SUPPLEMENTARY MATERIAL

The Supplementary Material for this paper is available online at https://dx.doi.org/10.2166/wst.2020.129.

REFERENCES

Bokare, A. D. & Choi, W. 2014 Review of iron-free Fenton-like systems for activating H_2O_2 in advanced oxidation processes. *Journal of Hazardous Materials* **275**, 121–135. https://doi.org/10.1016/j.jhazmat.2014.04.054.

Dong, J., Dong, H., Han, L., Fu, B., Chen, Y. & Zhan, Y. 2015 Peroxide degradation of azo dye using hydrothermally synthesized Cu-L zeolite as high performance catalyst. *Desalination and Water Treatment* **56** (4), 1056–1065. https://doi.org/10.1080/19443994.2014.941412.

Espinosa, J. C., Navalón, S., Primo, A., Moral, M., Sanz, J. F., Álvaro, M. & García, H. 2015 Graphenes as efficient metal-free Fenton catalysts. *Chemistry–A European Journal* **21** (34), 11966–11971. https://doi.org/10.1002/chem.201501533.

Granzier-Nakajima, T., Fujisawa, K., Anil, V., Terrones, M. & Yeh, Y. T. 2019 Controlling nitrogen doping in graphene with atomic precision: synthesis and characterization. *Nanomaterials* **9** (3), 425. https://doi.org/10.3390/nano9030425.

Gu, T., Dong, H., Lu, T., Han, L. & Zhan, Y. 2019 Fluoride ion accelerating degradation of organic pollutants by Cu(II)-catalyzed Fenton-like reaction at wide pH range. *Journal of Hazardous Materials* **377**, 365–370. https://doi.org/10.1016/j.jhazmat.2019.05.073.

Hammedi, T., Triki, M., Alvarez, M. G., Llorca, J., Ghorbel, A., Ksibi, Z. & Medina, F. 2019 Heterogeneous Fenton-like oxidation of p-hydroxybenzoic acid using Fe/CeO_2-TiO_2 catalyst. *Water Science and Technology* **79** (7), 1276–1286. https://doi.org/10.2166/wst.2019.119.

Kong, X. K., Chen, C. L. & Chen, Q. W. 2014 Doped graphene for metal-free catalysis. *Chemical Society Reviews* **43** (8), 2841–2857. https://doi.org/10.1039/C3CS60401B.

Kumar, S., Karthikeyan, S. & Lee, A. F. 2018 g-C_3N_4-based nanomaterials for visible light-driven photocatalysis. *Catalysts* **8** (2), 74. https://doi.org/10.3390/catal8020074.

Lee, H., Lee, H. J., Seo, J., Kim, H. E., Shin, Y. K., Kim, J. H. & Lee, C. 2016 Activation of oxygen and hydrogen peroxide by copper(II) coupled with hydroxylamine for oxidation of organic contaminants. *Environmental Science & Technology* **50** (15), 8231–8238. https://doi.org/1021/acs.est.6b02067.

Li, H. J., Sun, B. W., Sui, L., Qian, D. J. & Chen, M. 2015 Preparation of water-dispersible porous g-C_3N_4 with improved photocatalytic activity by chemical oxidation. *Physical Chemistry Chemical Physics* **17** (5), 3309–3315. https://doi.org/10.1039/C4CP05020G.

Liu, J., Zhang, T., Wang, Z., Dawson, G. & Chen, W. 2011 Simple pyrolysis of urea into graphitic carbon nitride with recyclable adsorption and photocatalytic activity. *Journal of Materials Chemistry* **21** (38), 14398–14401. https://doi.org/10.1039/C1JM12620B.

Lu, J., Wang, Y., Huang, J., Cao, L., Li, J., Hai, G. & Bai, Z. 2016 One-step synthesis of g-C_3N_4 hierarchical porous structure nanosheets with dramatic ultraviolet light photocatalytic activity. *Materials Science and Engineering: B* **214**, 19–25. https://doi.org/10.1016/j.mseb.2016.08.003.

Lyu, L., Zhang, L. & Hu, C. 2015 Enhanced Fenton-like degradation of pharmaceuticals over framework copper species in copper-doped mesoporous silica microspheres. *Chemical Engineering Journal* **274**, 298–306. https://doi.org/10.1016/j.cej.2015.03.137.

Mamba, G. & Mishra, A. K. 2016 Graphitic carbon nitride (g-C_3N_4) nanocomposites: a new and exciting generation of visible light driven photocatalysts for environmental pollution remediation. *Applied Catalysis B: Environmental* **198**, 347–377. https://doi.org/10.1016/j.apcatb.2016.05.052.

Martin-Martinez, M., Ribeiro, R. S., Machado, B. F., Serp, P., Morales-Torres, S., Silva, A. M. T., Figueiredo, J. L., Faria, J. L., Gomes, H. T. & Gomes, H. T. 2016 Role of nitrogen doping on the performance of carbon nanotube catalysts: a catalytic wet peroxide oxidation application. *ChemCatChem* **8** (12), 2068–2078. https://doi.org/10.1002/cctc.201600123.

Navalon, S., Dhakshinamoorthy, A., Alvaro, M., Antonietti, M. & García, H. 2017 Active sites on graphene-based materials as

metal-free catalysts. *Chemical Society Reviews* **46**, 4501–4529. https://doi.org/10.1039/C7CS00156H.

Ong, W. J., Tan, L. L., Ng, Y. H., Yong, S. T. & Chai, S. P. 2016 Graphitic carbon nitride (g-C_3N_4)-based photocatalysts for artificial photosynthesis and environmental remediation: are we a step closer to achieving sustainability? *Chemical Reviews* **116** (12), 7159–7329. https://doi.org/10.1021/acs.chemrev.6b00075.

Pisanu, A., Speltini, A., Vigani, B., Ferrari, F., Mannini, M., Calisi, N., Cortigiani, B., Caneschi, A., Quadrelli, P., Profumo, A. & Malavasi, L. 2018 Enhanced hydrogen photogeneration by bulk g-C_3N_4 through a simple and efficient oxidation route. *Dalton Transactions* **47** (19), 6772–6778. https://doi.org/10.1039/C8DT00276B.

Reddy, K. R., Reddy, C. V., Nadagouda, M. N., Shetti, N. P., Jaesool, S. & Aminabhavi, T. M. 2019 Polymeric graphitic carbon nitride (g-C_3N_4)-based semiconducting nanostructured materials: synthesis methods, properties and photocatalytic applications. *Journal of Environmental Management* **238**, 25–40. https://doi.org/10.1016/j.jenvman.2019.02.075.

Ribeiro, R. S., Silva, A. M., Figueiredo, J. L., Faria, J. L. & Gomes, H. T. 2016 Catalytic wet peroxide oxidation: a route towards the application of hybrid magnetic carbon nanocomposites for the degradation of organic pollutants. A review. *Applied Catalysis B: Environmental* **187**, 428–460. https://doi.org/10.1016/j.apcatb.2016.01.033.

Su, Z., Li, J., Zhang, D., Ye, P., Li, H. & Yan, Y. 2019 Novel flexible Fenton-like catalyst: Unique CuO nanowires arrays on copper mesh with high efficiency across a wide pH range. *Science of The Total Environment* **647**, 587–596. https://doi.org/10.1016/j.scitotenv.2018.08.022.

Sudhaik, A., Raizada, P., Shandilya, P., Jeong, D. Y., Lim, J. H. & Singh, P. 2018 Review on fabrication of graphitic carbon nitride based efficient nanocomposites for photodegradation of aqueous phase organic pollutants. *Journal of Industrial and Engineering Chemistry* **67**, 28–51. https://doi.org/10.1016/j.jiec.2018.07.007.

Vega, E. & Valdés, H. 2018 New evidence of the effect of the chemical structure of activated carbon on the activity to promote radical generation in an advanced oxidation process using hydrogen peroxide. *Microporous and Mesoporous Materials* **259**, 1–8. https://doi.org/10.1016/j.micromeso.2017.09.018.

Wang, X., Li, D. & Nan, Z. 2019 Effect of N content in g-C_3N_4 as metal-free catalyst on H_2O_2 decomposition for MB degradation. *Separation and Purification Technology* **224**, 152–162. https://doi.org/10.1016/j.seppur.2019.04.088.

Wu, D., Liu, Y., Zhang, Z., Ma, L. & Zhang, Y. 2015 Pyrite-enhanced degradation of chloramphenicol by low concentrations of H_2O_2. *Water Science and Technology* **72** (2), 180–186. https://doi.org/10.2166/wst.2015.202.

Yang, L., Huang, J., Shi, L., Cao, L., Yu, Q., Jie, Y., Fei, J., Ouyang, H. & Ye, J. 2017 A surface modification resultant thermally oxidized porous g-C_3N_4 with enhanced photocatalytic hydrogen production. *Applied Catalysis B: Environmental* **204**, 335–345. https://doi.org/10.1016/j.apcatb.2016.11.047.

Yue, X., Yi, S., Wang, R., Zhang, Z. & Qiu, S. 2016 Cadmium sulfide and nickel synergetic co-catalysts supported on graphitic carbon nitride for visible-light-driven photocatalytic hydrogen evolution. *Scientific Reports* **6**, 22268. https://doi.org/10.1038/srep22268.

Zhang, L., Xu, D., Hu, C. & Shi, Y. 2017 Framework Cu-doped $AlPO_4$ as an effective Fenton-like catalyst for bisphenol A degradation. *Applied Catalysis B: Environmental* **207**, 9–16. https://doi.org/10.1016/j.apcatb.2017.02.002.

Zhao, H., Wang, J., Zhang, D., Dai, Q., Han, Q., Du, P., Liu, C., Xie, Y., Zhang, Y., Cao, H. & Fan, Z. 2017 Chloro-benquinone modified on graphene oxide as metal-free catalyst: strong promotion of hydroxyl radical and generation of ultra-small graphene oxide. *Scientific Reports* **7**, 42643. https://doi.org/10.1038/srep42643.

Zhu, Y., Zhu, R., Xi, Y., Zhu, J., Zhu, G. & He, H. 2019 Strategies for enhancing the heterogeneous Fenton catalytic reactivity: a review. *Applied Catalysis B: Environmental* **255**, 117739. https://doi.org/10.1016/j.apcatb.2019.05.041.

First received 4 December 2019; accepted in revised form 15 March 2020. Available online 23 March 2020